Journal of CO_2 Utilization 34 (2019) 303–312

Contents lists available at ScienceDirect

Journal of CO_2 Utilization

journal homepage: www.elsevier.com/locate/jcou

Exploration of alkali cation variation on the synthesis of carbon nanotubes by electrolysis of CO_2 in molten carbonates

Xirui Wang, Xinye Liu, Gad Licht, Baohui Wang, Stuart Licht*

Department of Chemistry, George Washington University, Washington DC, 20052, United States

ARTICLE INFO

Keywords:
Carbon dioxide
Electrosynthesis
Molten salt
Carbon nanotube
Inconel

ABSTRACT

The electrochemical splitting of CO_2 in molten carbonate salt electrolytes can form a valuable product, carbon nanotubes, and with this product a value-incentivized pathway of climate change mitigation by transforming CO_2 from a greenhouse gas pollutant into a useful resource. Instability of the anode can provide a challenge for a commercialization of this electrochemical technology. A nickel superalloy (Inconel 718) anode is shown to be highly stable for the scalable controllable, electrosynthesis of nano-carbons from CO_2 in molten carbonates salts. Unlike pure nickel anodes that degrade (corrode) in the presence of potassium carbonate containing molten electrolytes, Inconel is stable as an anode even in these electrolytes. This opens up more cost-effective electrolytes (less expensive than lithium carbonate), and the systematic variation of alkali cation carbonates is explored. Coupled with a brass cathode, uniform carbon nanotubes (CNT) are efficiently synthesized by electrolysis of CO_2 in either pure Li_2CO_3 or in ternary electrolytes, Li_2CO_3-Na_2CO_3-$LiBO_2$ or Li_2CO_3-K_2CO_3-$LiBO_2$. These results increase the foundation of understanding of the electrolytic splitting of carbon dioxide and provide the data for developing a high-efficiency CO_2 electroreduction for the production of carbon nanotubes.

1. Introduction

Until the beginning of the Industrial Revolution atmospheric CO_2 concentration was stable at ~230 ± 50 ppm for the past 400,000 years. However concurrent with CO_2 release from fossil fuel combustion during the industrial age, this CO_2 concentration is rapidly increasing and the global CO_2 level has reached over 415 ppm as recorded in May 2019 (SCRIPPS UCSD). Unabated, atmospheric CO_2 might reach 500 ppm in the year 2060 [1]- - - This predominant greenhouse gas is a major cause of planetary climate change with consequences including the increasing probability of a climate induced extinction of - many of the species on the planet [2]. It is an urgent task for scientists and engineers to find a feasible industrial scale technology to capture and utilize CO_2.

One path to CO_2 removal from the carbon cycle is its transformation into stable, useful, valuable products. One allotrope of carbon, carbon nanotubes, has the highest tensile strength of all materials measured [3]. However, the common commercial form of carbon nanotube (CNT) production, chemical vapor deposition (CVD) is extraordinarily energy intensive and can emit over 600 tonnes of CO_2 per tonne of CNT produced [4,5]. Carbon nanotubes have been synthesized by several methodologies including flame, plasma and chemical vapor deposition CVD techniques [6–10]. CNT demand is mainly limited by the complexity and cost of those synthetic processes, which requires 30 to 100 fold higher production energy compared to aluminum [11–12]. As a result of the cost, energy intensity and complexity of the synthesis commercial CNTs currently are valued in the $100 K ($85–$450 K) per tonne range and do not use CO_2 as a reactant [10–13].

2. Experimental section

2.1. Experiment Preparation

Lithium carbonate (Li_2CO_3, 99.0%, Rockwood Lithium), sodium carbonate (Na_2CO_3, 99.98%, Sigma Aldrich), potassium carbonate (K_2CO_3, 99.95% Sigma Aldrich) and anhydrous lithium metaborate ($LiBO_2$, 99.9%, Alfa Aesar) are used as the electrolyte in this study. The electrolyte is pre-mixed in the ratio noted in Table 1. The 0.25-inch-thick brass sheet (purchased from onlinemetal.com) used as the cathode, and the 0.05-inch-thick Inconel 718 (purchased from onlinemetal.com) is used as the anode. Two sizes of electrodes are used in this study: 2 cm x 2.5 cm or 5 cm x 5 cm. The smaller electrolyses are - conducted in pure alumina tall form 100 ml crucible (AdValue 99.6% alumina), and the larger in a welded stainless steel 304 cell. An illustration of the reaction configuration is included in Fig. 1. Unlike nickel cells, which we've observed corrode and leak after 1 or 2 carbonate

* Corresponding author.
E-mail address: slicht@gwu.edu (S. Licht).

https://doi.org/10.1016/j.jcou.2019.07.007
Received 16 May 2019; Received in revised form 29 June 2019; Accepted 10 July 2019

Table 1
Electrolyte mixture composition as utilized for the alkali cation experiments.

Electrolyte Experiment Label	Li_2CO_3 (g)	Na_2CO_3 (g)	K_2CO_3 (g)	Extra $LiBO_2$ (g)
Li100	300	0	0	27
Na10	270	30	0	27
Na20	240	60	0	27
Na30	210	90	0	27
Na50	150	150	0	27
Na60	120	180	0	27
K20	240	0	60	27
K50	150	0	150	27

electrolyses, the 304 cells transform from a metallic to a black finish after a single electrolysis, which appears stable when used for repeated syntheses. Stainless steel 304 electrochemical cases have been used in more than 40 repeat syntheses without observation of any corrosion of the cell case.

2.2. Electrolysis and purification

Electrodes are perpendicularly immersed into the freshly made molten salt electrolyte with 1 cm separation. A constant current is applied at 0.2A/cm^2 for 4 or 5 h, at a voltage of 1–2 volts throughout the electrolysis, with the highest electrolysis potentials of up to 1.9 V observed only in the electrolytes containing 50% Li_2CO_3 or less (and either Na_2CO_3 or K_2CO_3). Electrolysis temperature is 740 °C. The raw product is collected from the brass cathode after the electrolysis is completed followed by an aqueous wash procedure. The washed carbon product is separated by vacuum filtration. The washed carbon product is dried overnight at 60 °C oven yielding a black power product.

2.3. Calculation

Considering the net reaction is [5]:

$$CO_2\ (gas) \rightharpoonup C\ (solid) + O_2\ (gas) \quad (7)$$

The Coulombic efficiency is calculated as Eq. (8):

$$Coulombicefficiency = 100\ \% \times \frac{C_{experimental}}{C_{theroretical}} \quad (8)$$

The $C_{experimental}$ is determined by mass of the dried final product mentioned in the previous section, and the following Eq. (9) to calculate the $C_{theoretical}$:

$$C_{theoretical} = \frac{Q}{nF} \times 12.01g \quad (9)$$

Where Q is the total electrolysis charged applied in As, F is the charge of one mole of electrons, 1 Faraday = 96485As, and the n is the - number of electron for the reduction of tetravalent carbon, 4.

2.4. Characterization

Samples are analyzed by PHENOM Pro-X Energy Dispersive Spectroscopy (EDS) on the PHENOM Pro-X SEM, and by FEI Teneo Talos F200XTEM.

2.5. Measurement of oxygen evolution during electolysis

The measurement of the gas product of CO_2 electrolysis in molten carbonate utilizes a sealed molten electrolysis with a gas input tube immersed in the electrolyte, two electrical connections respectively to the anode and cathode, and a gas output tube sitting in the head space above the molten electrolyte. The electrical connections passing through the cell cover were isolated by alumina tubing. The cell had an internal volume of 1069 ml including 120 ml of head space above 1670 g of molten Li_2CO_3 electrolyte. The planar, vertical anode and cathode were spaced 1.5–2 cm apart, and each had active (immersed) area of 80 cm^2. The electrolysis was conducted at 770 °C at a constant current of 12 A (a current density of 0.15 A cm^{-2}). CO_2 is fed into the gas input tube, and gas output CO_2 and O_2 composition was measured (subsequent to cooling in a long outlet tube) in real time during the electrolysis. CO_2 and O_2 composition was measured with digitially interfaced CO2meter.com sensors for CO_2 (CM-40801) and O_2 (CM-0160), and O_2 was redundantly measured with a WYF CY-12C oxygen meter.

3. Results and discussion

3.1. CO_2 molten carbonate electrolysis electrode stability

We recently discovered a high yield, high purity, (low) electricity cost constrained, synthesis of carbon nanotubes from CO_2 (the synthesis is termed C2CNT ≡ CO_2 to CNT) [13–15]. C2CNT splits carbon dioxide at by electrolysis in molten carbonates. The synthesis occurs as illustrated in the Fig. 1A:

$$Li_2CO_3 \rightarrow C_{CNT} + O_2 + Li_2O \quad (1)$$

CO_2 added to the electrolyte dissolves and chemically reacts with lithium oxide to renew and reform Li_2CO_3:

$$CO_2 + Li_2O \rightarrow Li_2CO_3 \quad (2)$$

Transition metals, such as Ni or Cr, nucleate CNT formation [13–15], comprise < 0.1% by mass of the product, and can be added to the electrolyte, to the cathode, or added by leach from the anode. The net reaction of Eqs. 1 and 2, is CO_2 split by electrolysis to carbon nanotubes and oxygen:

$$CO_2 \rightarrow C_{CNT} + O_2 \quad (3)$$

Physical chemical systems of CNT synthesis by conventional chemical vapor deposition are different in most aspects than that of the new C2CNT synthesis. The former is a chemical process, while the latter is an electrochemical process. CVD utilizes various organometallic forms as the reactant, while C2CNT utilizes CO_2, and CVD has a high carbon (positive) footprint while C2CNT has a carbon negative footprint. In general, CVD occurs at a gas/solid interface, while C2CNT occurs at the liquid/solid interface. In addition, there are significant mechanistic differences between CVD and C2CNT. With the C2CNT process the molten carbonate electrolyte is providing a higher density of reactive carbon sites (a high activity of tetravalent carbon available for reduction at the cathode) compared to a lower density of carbon available as a gas in CVD. An electric field may, or may not, be applied to the substrate during CVD CNT growth, During C2CNT growth, there is always an intense electric field rapidly decreasing through the double layer adjacent to the cathode. Isotopic ^{13}C tracking was used to follow CO_2's consumption as it is dissolved in molten carbonate and is split by electrolysis to form the building blocks of CNTs [14]. C2CNT transforms CO_2 to CNTs by molten electrolysis [13–22].

Transition metal nucleated electrolysis in lithium carbonate (pure or with added oxides [13,15,16], added sodium, calcium, or barium carbonates [20,22], or added boron, sulfur, phosphorus or nitrogen dopants [15,16,22]) forms carbon nanotubes, oxygen and dissolved lithium oxide. The CNT synthesis is linearly scalable with increasing electrode areas, and the CO_2 dissolution in molten lithium carbonate is exothermic and with electrolysis provides thermal balance [23]. Analogous to the case of the production costs of conventional aluminum smelting by electrolysis of the oxide (bauxite) in a molten salt, the cost of CNTs by electrolysis of carbon dioxide in a molten salt (molten carbonates) is only the order of $1000 per tonne [16].

Electrolysis temperatures lower than 700 °C or higher than 800 °C tend to form a lower fraction of carbon nanotubes in the carbon product

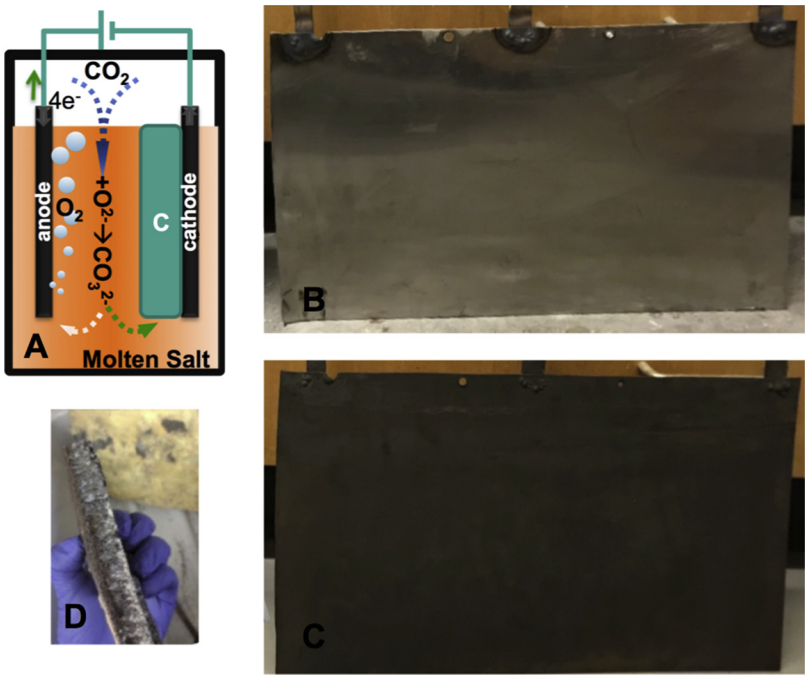

Fig. 1. The process of CO_2 electrolysis in molten carbonate (A) and the stability of the Inconel 718 anode and brass cathode after repeat and/or long duration. The 37.5 cm x 23 cm Inconel anode is shown new (B) and after its 12th electrolysis (C). The 37.5 cm x 23 cm brass cathode is shown (D, background) after its 4th electrolysis, and the cathode product from that electrolysis product is shown (D, foreground), which has snapped off as a single product "brick".

[24]. Inclusion of K_2CO_3 in the molten carbonate mix tends to corrode the nickel anode [23a], and platinum and iridium anodes, which can be stable are expensive [13,25]. In this study a durable, but not noble, anode is demonstrated that facilitates the use of a mixed molten carbonate in lieu of lithium carbonate, including mixed K/$LiCO_3$ electrolytes. Durability, lower cost electrolyte (potassium or sodium carbonate is significantly less expensive than lithium carbonate), and the lower viscosity of a binary or ternary, compared to unary carbonate electrolyte [26,27] are each advantages for a sustainable, scalable and controllable electrosynthesis of nano-carbon from atmospheric CO_2.

Nickel alloys including Nichrome (Chromal) and Inconel 600, 625 and 718 each are stable as anodes during the extended electrolytic splitting of CO_2 electrolyses in molten carbonate. Inconel 718 alloy is composed of nickel (50–55 wt %) and chromium (17–21%) and molybdenum (2.8–3.3%) plus significant amounts of iron, columbium, and molybdenum [17]. This study presents the use of Inconel 718 as a C2CNT process anode, although we have found that Inconel 625 is also widely effective. However, Inconel 625 contains higher nickel (> 58%) chromium (20–23%) and molybdenum (8–10%) and less iron than Inconel 718. Additionally, Inconel 718 contains higher niobium and tantalum (4.7–5.5%) than Inconel 625 (3.1–4.2%). Inconel 718 is readily available, has high physical strength and corrosion-resistant properties and is economical. Fig. 1 illustrates CO_2 electrolyses in molten carbonate and presents the stability of the Inconel 718 anode both before (Fig. 1B) after both repeat and/or long duration (Fig. 1C). The Inconel 718 anode remained a uniform dark grey and did not display any indication of corrosion throughout over a dozen separate electrolyses varying in duration from 4 to 72 h. Cumulatively, the experiments demonstrate a stable superalloy anode with extensive durability sustained during electrolysis in a variety of electrolytes during accumulated electrolyses of over 200 -hs operation.

The brass (copper/zinc) cathode used in the current study is conducive to long CNTs and is shown in the background of Fig. 1D after its 4th electrolysis. The cathode product is shown in the foreground of Fig. 1D after a 72 h electrolysis, and subsequent to extraction and cooling, snaps off as a single "brick". There is no indication or coloration of brass on the brick, and the cathode is reused after the visible small residual carbon product observed in the figure is removed.

3.2. Oxygen evolution during CO_2 molten carbonate electrolysis

The consumption of the greenhouse carbon dioxide by molten carbonate electrolytic splitting forms two simultaneous products. In addition to solid carbon, the second product of CO_2 electrolysis is O_2, and the evolution of pure oxygen during the electrolysis is demonstrated here. CO_2 added to the electrolyte dissolves and chemically reacts with lithium oxide to renew and reform Li_2CO_3. The net reaction of eqs 1 and 2 is CO_2 split by electrolysis to carbon and oxygen in accord with Eqs. 1 to 3.

The measurement of the gas product of CO_2 electrolysis in molten carbonate utilizes a sealed molten electrolysis with a gas input tube immersed in the electrolyte, two electrical connections respectively to the anode and cathode, and a gas output tube sitting in the head space above the molten electrolyte as shown in Fig. 2 left and middle photographs.

The measured oxygen (and carbon dioxide composition) of the output gas during two electrolyses is reported in the right side of Fig. 2. The first is conducted in a Li_2CO_3 electrolyte, and the second in Li_2CO_3 containing 1 m Li_2O. As seen in the figure the oxygen composition of the gas rises as the 21% oxygen in the initial air in the headspace is replaced with the electrolyzed gas product, and approaches 100% oxygen as electrolysis progresses. Unlike all the other experiments in this study which uses real air (direct air carbon capture with 400–500 ppm CO_2), in these experiments to demonstrate and emphasize the high purity O_2 co-produced in CO_2 electrolysis, pure CO_2 is fed as the only inlet gas into the cell at a rate equivalent to the applied electrolysis current (CO_2 inlet rate = 44.9 ml per minute = 12 A applied electrolysis, at 4 Faraday per mole CO_2 reduction). In accord with eq. 2, lithium oxide is regeneratively consumed to capture carbon dioxide and reform the lithium carbonate electrolyte. As seen in the figure, initially (peaking in the first 10 min) inlet CO_2 partially escapes, and then CO_2 concentration in the outlet gas rapidly diminishes and approaches 0%. We have previously observed that molten Li_2CO_3 requires a few hours to reach an equilibrium concentration of 0.3 molal Li_2O (moles per kg Li_2CO_3), and attribute this initial buildup to the (i) time needed for this equilibration and (ii) time needed for oxide formed by electrolysis at the electrodes in accord with eq. 1 to reach the bulk electrolyte (and react with CO_2).[44] In the second experiment, when the initial electrolyte is 1 molal $L_{i2}O$ (rather than pure Li_2CO_3), less initial CO_2 release

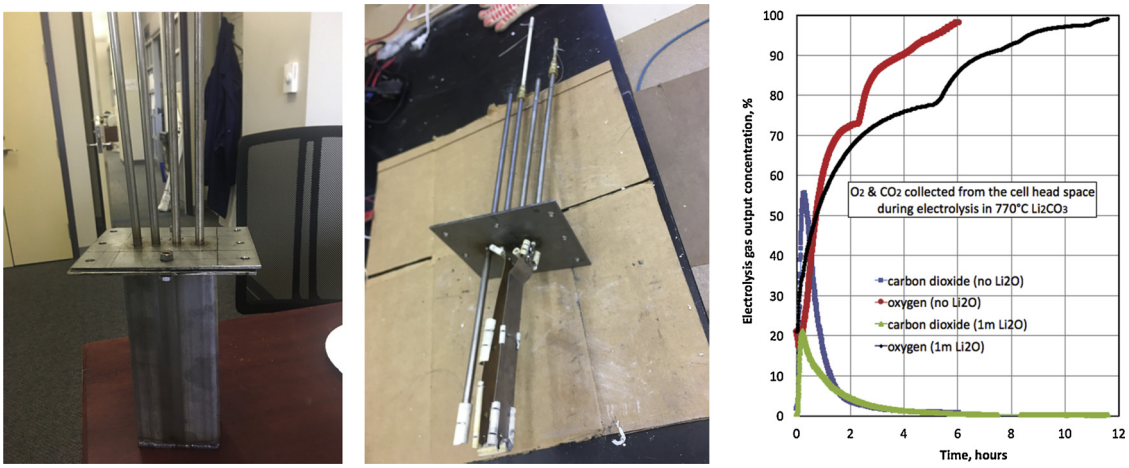

Fig. 2. Oxygen evolution during CO_2 molten carbonate electrolysis. Left: Electrolysis cell. Middle: Cover, gas inlet and exit, electrical connections, and electrodes prior to immersion in electrolyte with or without added Li_2O, and cell sealing. Right: Oxygen (red or black curves) and carbon dioxide (blue or green) composition of the output gas during the electrolysis.

occurs, and again the outlet gas rapidly builds to pure oxygen.

The second product of the C2CNT process (in addition to carbon nanotubes) hot oxygen is useful in a range of industrial and manufacturing processes [28–38]. Compared to air, oxygen improves the efficiency and concentration of ozone generation [28] and is an essential feedstock in the manufacture of a variety of industrial chemical and monomers. These include TiO_2 production, ethylene and propylene oxides, acetaldehyde, vinyl chloride or acetate, and caprolactam productions [20–30]. Using oxygen in lieu of air consumes proportionally less fuel or generates a higher combustion temperature. For example, for air compared to oxygen methane combustion the ignition temperature decreases from 632 °C (air) to 536 °C (oxygen), and the adiabatic flame temperature increases from 1950 °C to 2780 °C [29]. As reported by Hendershot et al, from an energy efficiency perspective, the nitrogen and argon in combustion are detrimental. N_2 and Ar amount to about 79% of on a molar basis, do not aid in the process, but must still be heated to the same temperature as the combustion products [30]. Not all of the flue gas enthalpy can be recovered and exhausting these gases involves an inherent loss of energy. Limiting the amount of nitrogen in the process permits the use of smaller, less-expensive equipment, and the overall flow is lower than that of air-based process, which minimizes pressure drops in air-handling equipment [18]. The generated O_2 product is useful in various applications as an oxy-fuel to decrease total CO_2 in industrial process while enriching relative CO_2 levels in flue gas CO_2 [31–36]. The “oxy-fuel” replacement of air by hot oxygen realizes a fuel savings of 25–60% [29]. In some industries the

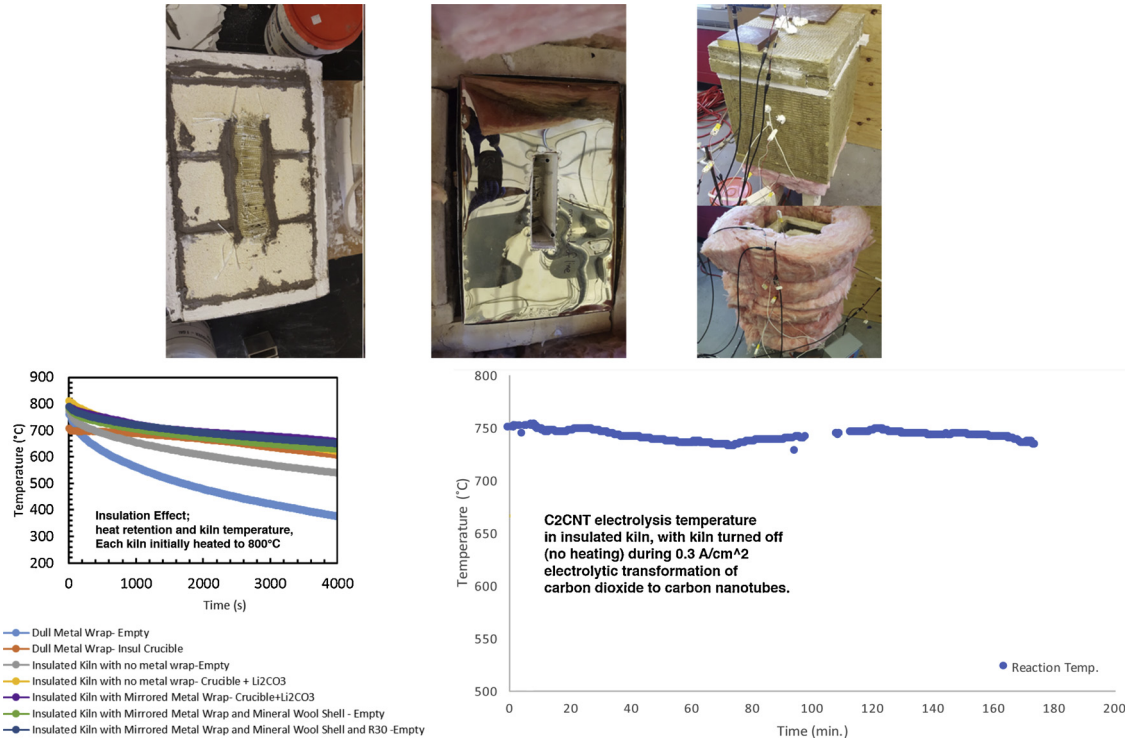

Fig. 3. The performance of a custom-built kiln increasingly retains heat as various indicated thermal insulation and radiative reflective layers are added.
Top: A kiln with custom thermal insulating layers was used to test thermal conservation of the C2CNT process. Bottom Left: The kiln’s ability to retain temperature as measured by thermocouple, subsequent to an initial heating to 800 °C, and with various indicated thermal insulation barriers. Bottom right: With all thermal layers in place, the electrolytic splitting of CO_2 by molten carbonate electrolysis maintains a constant temperature without external heating.

replacement of air with oxygen has already been implemented, for example in the glass production industry due to the need to reach higher melt temperatures [32], while in other industries such as cement and steel this replacement has been hindered by the high dollar and energy cost of separating oxygen from the air [33–36]. The fuel savings by retrofitting air/fuel systems with oxy/fuel is 40–60% for the steel and copper industries, 50% for waste incineration and sulfuric acid recovery, 40% for the aluminum and lead industries, and 30–40% for the glass industry [29,37].

Here, molten carbonate electrolysis offers a novel source for energetic (hot) oxygen production. In the early 1900's cryogenic air separation started at an industrial scale. Today oxygen is conventionally produced principally by cryogenic cooling, and to a lesser extent by membrane and adsorption technologies [38]. Pure oxygen separation from air requires a thermodynamic energy of 53.1 kW h/tonne, and practical energy of 196 kW h / tonne oxygen [39–41].

3.3. Thermal balance during molten carbonate electrolysis

The dissolution of carbon dioxide in molten lithium carbon is exothermic and rapid, which along with the heat generated by the electrolysis, provides thermal balance. A critical thermal balance breakthrough was reached in which the C2CNT process requires no external heating. C2CNT is a high temperature process. However, with appropriate insulation the electrolysis is self-heating and does not require external heating after the initial molten, as shown in Fig. 3. As seen in the top of the figure one inch thick, rigid McMaster 6841K5 insulation was used as a thermal barrier (K = 0.28 at 800 °C) and placed adjacent to the thermally insulating BNZ kiln firebricks. This rigid insulation barrier is visible as the outer white edge in addition to the grey furnace mortar and bricks, on the left side photo. In the middle top photo an added mirror-reflective 304 stainless steel barrier is visible as thermal radiative battier. A 4th layer of thermal insulation (in addition to the firebrick, radiative barrier and ceramic insulation) was added as mineral wool insulation, yellow-green as seen in the right-top photo (McMaster no. 9328K43), and the 5th visible outer coating of pink R-30 insulation was added as a final insulation. The cover is removed and the C2CNT CO_2 to carbon nanotube electrolysis chamber is placed inside.

With all thermal layers in place, the electrolytic splitting of CO_2 by molten carbonate electrolysis maintains a constant temperature without external heating as shown on the right side of Fig. 3. C2CNT is conducted at constant current in the insulated kiln. At an electrolysis current density, J = 0.1 cm^{-2} the cell maintained a constant temperature of 727 °C. As shown at J = 0.3 cm^{-2} the cell maintained a constant temperature of 750 °C at (a poor thermocouple connection was corrected at 100 min); this experiment uses two internal C2CNT electrochemical cells connected in series, with a constant, equivalent CO_2 flow into the cell, and the electrolysis potential measured is 2.2($\pm$0.2)V throughout the electrolysis. The temperature increased to 787 °C when the current density and (proportional CO_2 flow rate) is increased to J = 0.5 A cm^{-2}. On the left side of Fig. 3, the kiln's partial ability to retain temperature is shown with the electrolysis off, but with an increasing number and type of insulation layers. In each measurement, subsequent to an initial heating to 800 °C, the kiln is turned off, and the internal temperature measured. It is seen that successive added thermal insulation barriers provide an increasing, high level of temperature stability.

3.4. Carbon nanotube growth during CO_2 molten carbonate electrolysis

Using Scanning Electron Microscopy (SEM) and Transmisson Electron Microscopy (TEM) images we probe the morphologies of carbon nanotubes produced by molten carbonate synthesis as they develop and become more distinct in time. As shown in Fig. 4 the carbon nanostructures evolve from an indistinct Ni nucleated carbon nano-onion/carbon nanotube mix (Figs. 4A) to a pure carbon nanotube product in the first minutes of electrolysis. With extended electrolysis time the product quickly resolves into pure carbon nanotubes (Fig. 4B and 4C). The number of CNT walls and diameter increasing with increasing electrolysis time. For example, on the copper cathode, as shown in Figs. 4C, after 90 min the carbon nanotube has 142 distinct walls (compared to 18 and 39 walls respectively after 25 and 30 min) separated by an interlayer separation of 3.35 nm typical of graphitic strutures.

3.5. Effect of cation variation on CO_2 molten carbonate electrolysis

To understand durable anode, electrolyte and carbon nanotube product effects, we systematically designed a series of experiments using a superalloy Inconel 718 anode with a varied proportion of Li_2CO_3, Na_2CO_3, and K_2CO_3 in the electrolyte. From the images of the Scanning Electron Microscopy (SEM) image and Energy-dispersive X-ray Spectroscopy (EDS), we determined the morphologies of nanotubes produced by the controlled, logical sequence of syntheses with compositional variations of the electrolyte containing diminished lithium content, lower melting temperature carbonate molten salts coupled with use of the superalloy anode. This study demonstrates the Inconel 718 superalloy plus lower lithium content and lower viscosity carbonates are a suitable candidate for the exploration of scalable CO_2 to CNT production enhancing this molten salt CO_2 capture and conversion technology to accelerate deployment and wide-scale usage.

The electrolysis configuration is detailed in our previous reports [15,16]. The Inconel anode and brass cathode used have a planar sheet morphology. As previously noted the molten electrolyte is allowed to reach a steady state equilibrium (pre-equilibration step) for 24 h prior to immersion of the electrodes [15]. Small scale 2 cm x 2.5 cm brass cathode and Inconel 718 anode were spaced 1 cm apart in the electrolyte in an alumina (Al_2O_3) crucible cell in the molten 24 h aged "pure" Li_2CO_3 electrolyte. A constant 1.00 A (0.200 A cm^{-2}) is applied for 5.00 h. After the synthesis, an approximately 1 cm thick, black product was formed on the surface of the cathode and was easily peeled off the cathode after cooling. The electrolysis time is chosen such that the cathode deposit approaches, but does not contact, the anode. The surface of the metal cathode was smooth after product peel, and bore a metallic luster without corrosion. After washing and drying, a fluffy black powder is obtained. The final product was weighed (0.56 g) for the coulombic efficiency calculation (= 100%); as determined from the 5 Ah of charge passed during the electrolysis. The SEM images as shown in Fig. 5 demonstrate that the formed carbon materials exhibit a uniform carbon nanotube morphology growing outward from an adjacent thin, shiny carbon sheet (located on the cathode side contact of the produce), observed as a shiny bottom layer of the product.

The product (other than a low level of carbon nanionions and carbon platelets from which CNT growth initiates) is pure carbon nanotubes. The carbon nanotubes seem to be composed of two varieties (i) ~80% of the CNTs, those grown in the front (near anode) regions of the cathode have an average diameter of 200 nm diameter and length of 200 μm (Fig. 5 A, B); (ii) while the remaining ~20% of the CNTs, those grown on the back edge of the cathode (the small surface area of the electrodes, makes the path length to the anterior cathode region viable) have an average diameter of 500 nm diameter and length of 200 μm long and length of 100 μm (Fig. 5 C, D). TEM of a separated anterior carbon nanotube from the Fig. 5 panels A and B product is presented in Fig. 6.

Experiments with other carbonate based electrolytes were conducted to investigate the suitability of these alternative electrolytes, and cation effects on the efficiency and morphology of C2CNT syntheses by decreasing the lithium ion content of carbonate mixtures of Li_2CO_3, Na_2CO_3 and K_2CO_3. In addition, we have previously determined through a series of measurements that the addition of 8 to 9 wt% metaborate, as $LiBO_2$ further improves the CNT product's electrical conductivity from 1.2 × 10^4 to 1.2 × 10^5 S m^{-1} without adverse

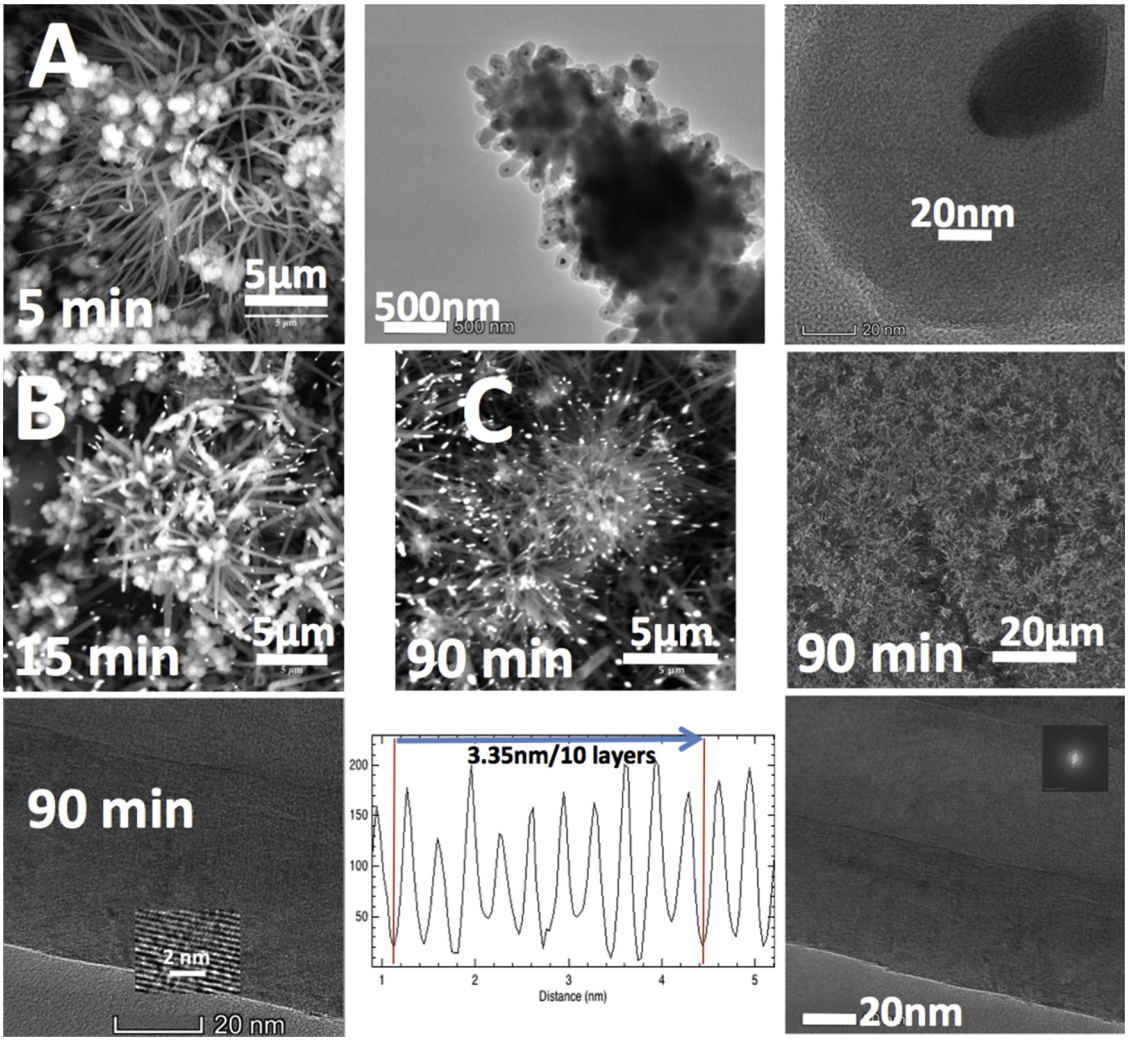

Fig. 4. CO_2 electrolysis in molten carbonate drives carbon nanotube growth on a copper cathode. electrolyses of various durations The electrolysis is conducted in 770 °C Li_2CO_3 at a constant current density of 0.2 A cm^{-2} then extracted and is washed of excess electrolyte. A: SEM and TEM of the product after 5 min of electrolysis, B: SEM after a 15 min electrolysis. C: SEM and TEM of the product after 90 min of electrolysis. Bottom: 90 min electrolysis interspatial graphene layer between the individual CNT walls.

effect on the CNT morphology, and this was added to all subsequent electrolytes. Detailed compositions of the alternative electrolytes that are compared are listed in Table 1. These experiments were carried out in the small prototype scale cell equipped with a larger 5 cm x 5 cm size of electrodes as compared in the lower portion of Fig. 5. A constant 5.0 A (0.200 A cm^{-2}) is applied for 4.00 h. The gap between anode and cathode remained 1 cm. The large difference in anode stabilities is evident when comparing electrolyses with a pure nickel versus an Inconel 718 anode. In experiments with Table 1's Na20 electrolyte (20 wt % Na_2CO_3 in Li_2CO_3), a pure nickel anode (rather than Inconel) anode broke at the liquid/air line after 30-min electrolysis. While highly stable in lithium carbonate electrolytes, nickel anodes tend to corrode into molten sodium and potassium carbonate mix, observable as a green coloration developing in the electrolyte during extended electrolyses. During the electrolysis, nickel oxide dissolves into the electrolyte as evidenced by x-ray powder diffraction of the electrolyte, subsequent to the electrolysis, which exhibits nickel oxide, and of the cathode product which contains nickel metal (presumably as reduced from the dissolved nickel oxide in the electrolyte) [23a]. In comparison, the Inconel 718 maintained its original shape and function in the above conditions, and in 100 -hs continuous run illustrated that neither visible distortion nor significant material lost were observed. The Inconel 718 anodes can be recycled in highly efficient electrosynthesis. Similar to the smaller scaled experiments, the synthesized product at a constant current density of 0.2A cm^{-2} of 5 h was approximately 1 cm thickness on the cathode, and again the electrolysis time has been chosen such that the cathode deposit approaches, but does not contact, the anode.

The C2CNT coulombic efficiencies, comparing the mass of the product to the applied $4e^-$ per mole of charge, approach 100% (98–100%) for the three cases of the Li100, Na10 (10% Na_2CO_3), and Na20 electrolyte experiments. Coulombic efficiency is still high, but decreased in binary lithium carbon electrolytes containing over 20% of sodium or potassium carbonate. For example, the coulombic electrolysis efficiency drops from 95% for Na30 electrolyte, to 93% Na50 electrolyte, to 90% for Na60 electrolyte. The coulombic efficiency drop is more rapid with an increasing fraction of potassium carbonate electrolyte, decreasing from 85% for the electrosynthesis in the K20 electrolyte to 79% for K50. We suggest that these measured coulombic efficiency drops are due to competing factors. We have calculated that the thermodynamic potential for the reduction of the alkali carbonates increases in the order $E_{Li2CO3} < E_{Na2CO3} < E_{K2CO3}$ [25]. The higher voltage of an increasing concentration of the latter salts would increase the possibility for reduction of the alkali cation to the alkali metal, rather than the desired reduction of carbonate to carbon. Alternatively, the increasing concentration of the secondary binary components will lower the electrolyte viscosity [26,27], which can facilitate carbon

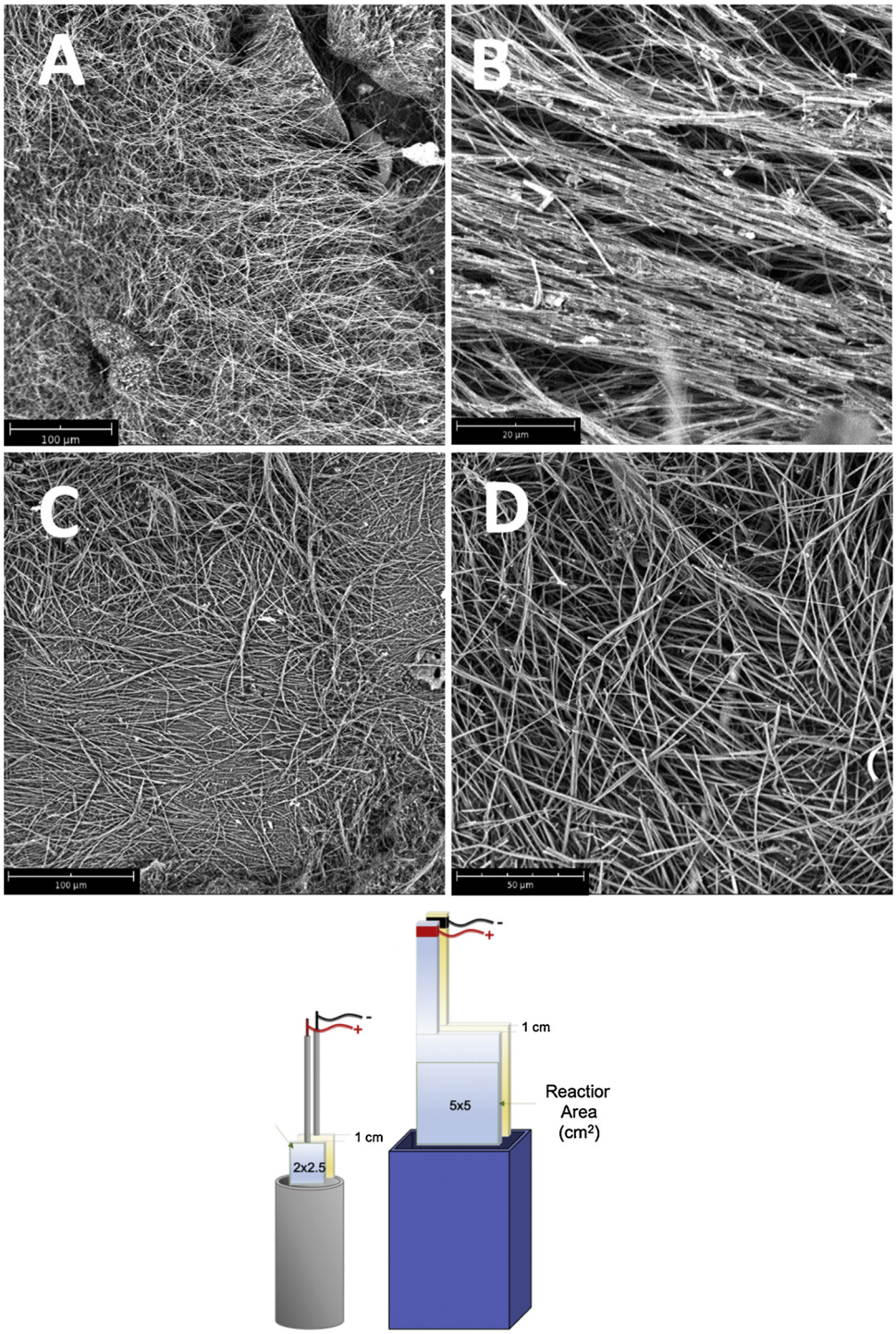

Fig. 5. Top: SEM images of carbon nanotube cathode product from electrolysis of 5 cm^2 Inconel 718 anode and brass cathode in 24-hr equilibrated Li_2CO_3 electrolyte housed in an alumina crucible. The size bars are 100 µm in both panels A and C, and are respectively 20 and 50 µm in panels B and D. As illustrated in the lower left corner, the cathode product in subsequent syntheses is grown by electrolysis with larger (25 cm^2) brass and Inconel electrodes, in a rectangular 304 stainless steel case, rather than in a tall form alumina crucible.

formation. However, the observed result is a clear trend of a modest decrease in carbon reduction coulombic efficiency with greater than 20 wt% of the non-lithium carbonate binary carbonate component.

Inclusion of $LiBO_2$ to the carbonate electrolyte affects carbon nanotube conductivity and morphology [15,16,22b]. Pure B_2O_3 (mp 450 C, white, melts clear) and the melt is a glass insulator. However, when molten B_2O_3 contains dissolved Li_2O (mp 1438 °C, white, melts clear) it becomes an electrochemical conductive liquid, dissolving as lithium metaborate, $LiBO_2$, which we have previously explored as a molten air battery electrolyte, and noted the phase diagram of mixed boron oxide and lithium oxide [42]. We have also previously noted that beyond 10% addition of lithium metaborate to molten lithium carbonate, the electrolyte becomes viscous impairing electrolytic CO_2 splitting and carbon nanotube formation [22b]. The study here uses a constant lithium metaborate concentration in the electrolyte (27 g in 327 g) to take advantage of the improved morphology observed with borate addition, while systematically exploring alkali cation variation effect on the synthesis. With inclusion of the $LiBO_2$ salt, the CNTs SEM images of the

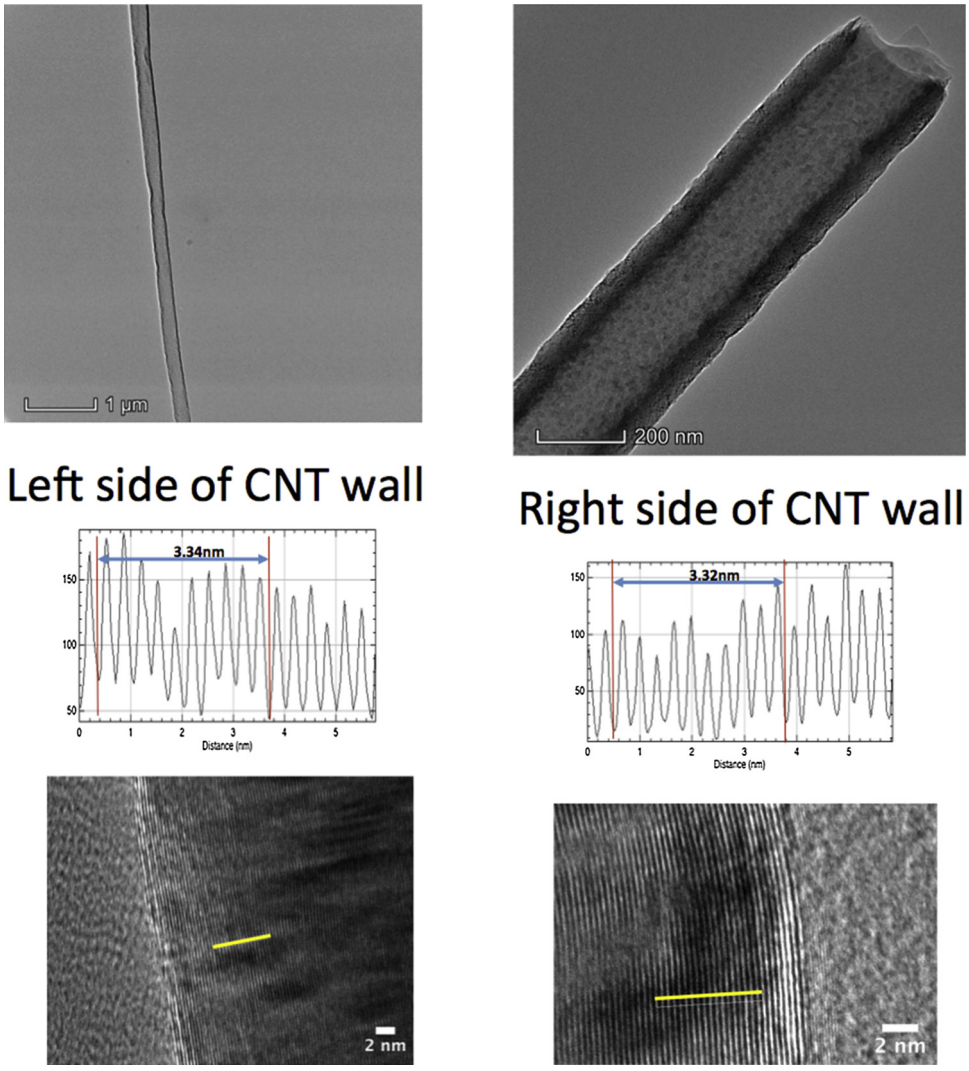

Fig. 6. Left and Right wall TEM of the cathode nanotube product from electrolysis of 5 cm^2 Inconel 718 anode and brass cathode in 24-hr equilibrated Li_2CO_3 electrolyte housed in an alumina crucible as shown by SEM in Fig. 5A and 5B including interspatial graphene layer between the individual CNT walls.

Li100 electrolyte electrolysis product exhibit thinner and shorter (50 nm thick and 20 μm long) morphology. SEM characterizations of the carbon nanotube product with electrolyte variation is shown in Fig. 7 and exhibits distinct morphological changes. CNTs such as in Fig. 7 panels A, C and D are less tangled and more aligned, while in electrolytes containing higher fractions of Li_2CO_3, the CNTs are more agglomerated and assembled as a tangled bundle shape in a series of increasing Na_2CO_3 fraction electrolyte experiments.

CNTs dimension have a larger diameter with increasing Na_2CO_3 percentage in the electrolyte (Na10: ~80 nm, Na20: ~100 nm, Na30: ~200 nm, Na50: ~1 μm). In the higher percentage of Na_2CO_3 (Na30 (not shown), Na50, and Na60) synthesis, fewer straight CNTs are evident. The Na20 CNTs are uniform and pure, while Na30, Na50 and Na50 exhibit an increasing fraction of non-CNT morphologies. Na60 consists of ~half platelets and half CNTs. Of the electrolytes compared, Na20 is favored when a straight, thin CNT product with high aspect ratio (~100 nm diameter, ~80 μm long) is desired. At higher weight fractions of Na_2CO_3 in the electrolyte, the majority of the product consists of thick, curled CNTs, accompanied by an increasing fraction of carbon nanospheres and carbon platelets. We have previously observed that curled CNTs are accompanied by a relative height increase in the D compared to G peaks in the Raman spectra, which is evidence of increased occurrence of sp^3 defects in the sp^2 wall structure [15]. In an expanded study, Raman defect spectra will be included. For the K20 (20 wt% K_2CO_3 in Li_2CO_3, SEM shown Fig. 7, Panel E) and K50 (not shown) electrolyses the loss of aspect ratio and increased twisting occurs more rapidly with increasing K_2CO_3 weight fraction than the electrosynthesis with increasing Na_2CO_3 fraction. Straight CNTs were uncommon in both products, particularly, the K50 case. Energy-dispersive X-ray spectroscopy (EDS) tests were employed to probe the elemental analysis of products from the Na20, 50Na, K20, and K50 cases. EDS of both the Na20 and K20 samples are 100% carbon, while the Na50 and K50 spectra are respectively 97.0% carbon (and 3.0% Na) and 97.8% carbon (and 2.2% K); boron in the CNTs is below the limits of EDS detection and we have previously employed Raman peak shift to quantify the extent of boron doping [22b].

A uniform carbon nanotube morphology can be obtained by electrolysis in molten carbonates. It is evident in Figs. 5 and 7 that the morphology varies with the composition of the alkali carbonate electrolyte. Binary and ternary carbonates have a lower viscosity than unary carbonates [26,27], which will increase ion mobility and mass diffusion, and addition of Na_2CO_3 and K_2CO_3 can increase the thermodynamic potential for alkali carbonate reduction. As we have previously measured, the reaction of carbon dioxide with solution phase oxide in molten lithium carbonate is rapid and exothermic [23b]. Peeters et al. have shown that this solubility may be even greater in mixed, compared to unary molten lithium carbonates [43]. In an expanded study we will attempt to isolate the magnitude of these factors

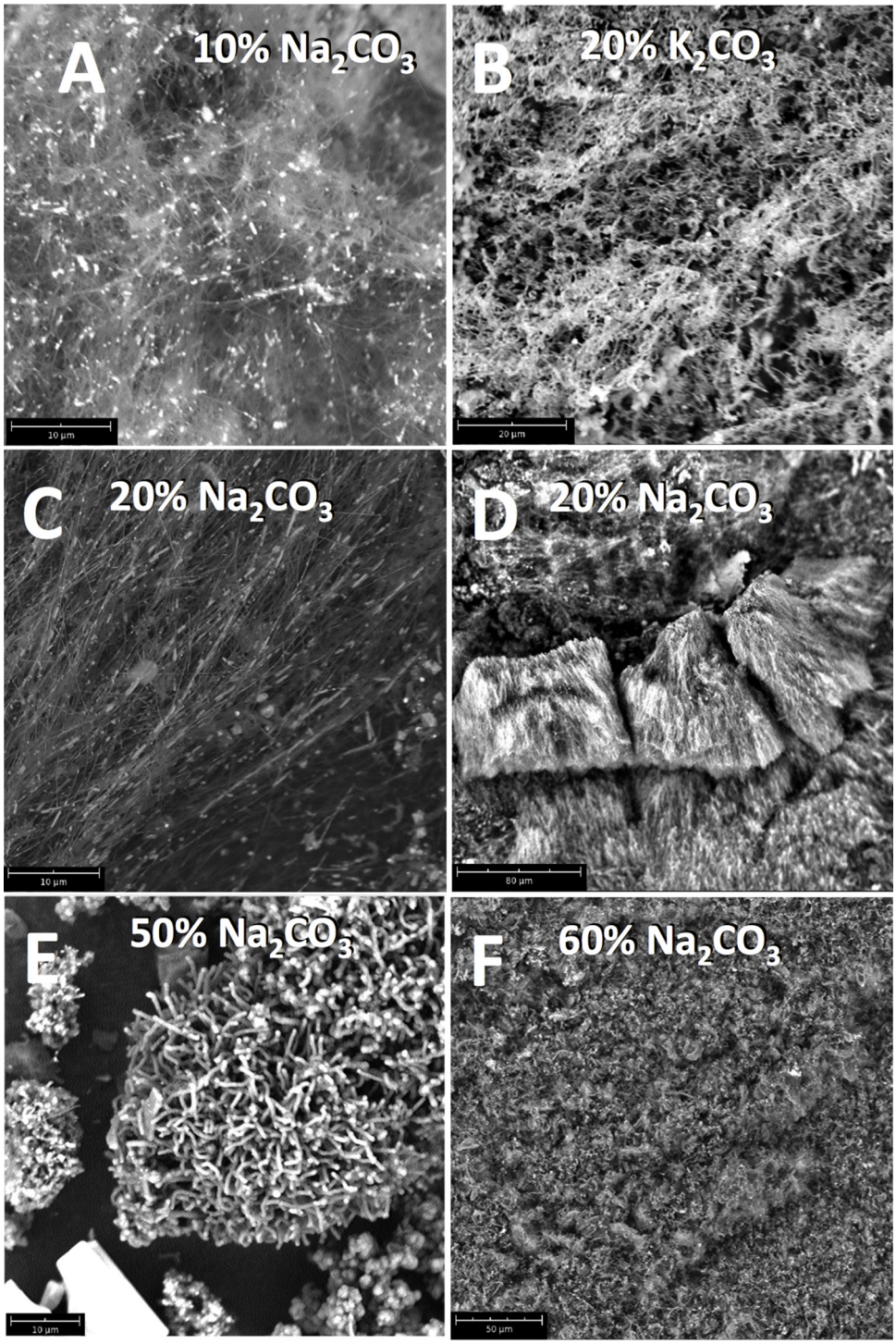

Fig. 7. Various Li_2CO_3 mixed electrolyte electrolyses conducted with larger 25 cm^2 electrodes and containing an additional 27 g $LiBO_2$. SEM image of washed carbon nanotube product obtained from Na10 electrolysis **A** (10 µm scale bar SEM); from K20 electrolysis **B** (20 µm scale bar SEM); from Na20 electrolysis panel **C** (10 µm scale bar SEM) & **D** (80 µm scale bar SEM); Na50 electrolysis **E** (10 µm scale bar SEM); Na60 electrolysis **F** (50 µm scale bar SEM).

on the cathode carbon nanomaterial product.

4. Conclusions

A nickel superalloy anode (Inconel 718) is a durable, cost effective anode for the electrolytic splitting of carbon dioxide in molten carbonate. The enhanced durability of this anode, and in the lack of corrosion previously observed at a nickel anode during electrolyses in potassium carbonate containing electrolytes, opens the path to the exploration of mixed carbonate electrolytes for the transformation of CO_2 to carbon nanotube products. Electrolyses in lithium carbonates mixed with either sodium or potassium carbonate produce carbon nanotube produces, and in particular an electrolyte containing an 80:20 mass ratio of lithium to sodium carbonate and mixed lithium metaborate was found effective in producing high purity, high aspect ratio carbon nanotubes at a high coulombic efficiency.

Declaration of Competing Interest

The authors declare no conflict of interest.

Acknowledgements

We are grateful to the Carbon XPrize and C2CNT for partial support of this research, and to Dr. Jason Lau and Juan Vicini who under the direction of SL were instrumental to the thermal balance measurements.

References

[1] S.J. Davis, K. Caldira, H.D. Mathews, Science 329 (2010) 1330.
[2] J.L. Penn, C. Deutsch, J.L. Payne, E.A. Sperling, Science 362 (2018) 1113.
[3] F. Li, H.M. Cheng, S. Bai, G. Su, M.S. Dresselhaus, Science 287 (2000) 637.
[4] V. Khanna, B.R. Bakshi, L.J. Lee, J. Ind. Ecology 1 (2010) 2363.
[5] O.G. Griffiths, J.P. O'Byrne, L. Torrente-Murciano, M.D. Jones, D. Mattia, C. Marcelle, Manus Mc, J. Cleaner Production 42 (2013) 180.
[6] (a) S. Iijima, Nature 354 (1991) 56;
(b) T.W. Ebbesen, P.M. Ajayan, Nature 358 (1992) 220;
(c) W.K. Hsu, J.P. Hare, H.W. Terrones, D. Kroto, R.M. Walton, Nature 377 (1995) 687.
[7] D. Janas, K.K. Koziol, Nanoscale 8 (2016) 19475.
[8] A. Magrez, S. Arnaud, J. Won, R. Smajda, et al., Materials 2 (1995) 4878.
[9] X.L. Jia, F. Wei, Top. Curr. Chem. (2017) 375, https://doi.org/10.1007/s41061-017-0102-2.
[10] Cheaptubes.com. Cheaptubes: Industrial Grade Carbon Nanotubes, (2017) Available from: http https://www.cheaptubes.com/product-category/industrial-carbon-nanotubes-products/.
[11] pluscomposites, Composites: Materials of the Future: - Part 4: Carbon Fibre Reinforced Composites, (2015) pluscomposites.eu/publications, at: http://www.pluscomposites.eu/sites/default/files/Technical%20series%20-%20Part%204%20-%20Carbon%20fibre%20reinforced%20composites_0.pdf.
[12] H.C. Kim, V. Fthenakis, Prog. Ind. Ecol. Int. J. 17 (2012) 528.
[13] J. Ren, F.-F. Li, J. Lau, L. Gonzalez-Urbina, S. Licht, Nano Lett. 15 (2015) 6142.
[14] J. Ren, S. Licht, Scientific Reports- Nature.com 6 (2016) 27760 1.
[15] M. Johnson, Ren J, M. Lefler, G. Licht, J. Vicini, X. Liu, S. Licht, Mater. Today Energy 5 (2017) 230.
[16] M. Johnson, Ren J, M. Lefler, G. Licht, J. Vicini, S. Licht, Data Brief 14 (2017) 592.
[17] S. Licht, A. Douglas, J. Ren, R. Carter, M. Lefler, C. Pint, ACS Cent. Sci. 2 (2015) 162.
[18] J. Ren, J. Lau, M. Lefler, S. Licht, J. Phys. Chem. C 119 (2015) 23342.
[19] G. Dey, J. Ren, T. El-Ghazawi, S. Licht, RSC Adv. 6 (2016) 27191.
[20] H. Wu, Z. Li, D. Ji, Y. Liu, L. Li, D. Yuan, Z. Zhang, J. Ren, M. Lefler, B. Wang, S. Licht, Carbon 106 (2016) 208.
[21] J. Lau, G. Dey, S. Licht, Energy Convers. Manage. 122 (2016) 400.
[22] (a) S. Licht, et al., J. CO_2 Utilization 18 (2017) 378;
(b) S. Licht, et al., J. CO_2 Utilization 18 (2017) 335;
(c) S. Licht, et al., J. CO_2 Utilization 12 (2013) 58.
[23] (a) S. Licht, Stabilization of STEP Electrolyses in Lithium-free Molten Carbonates. arXiv:1209.3512v1, (2012);
(b) S. Licht, Carbon Dioxide to Carbon Nanotube Scale-up. arXiv:1710.07246v1, (2017).
[24] (a) F.-F. Li, J.Lau S. Licht, Adv. Sci. 5 (2015) 1500260 1;
(b) F.-F. Li, S. Liu, B. Cui, J. Lau, J. Stuart, B. Wang, S. Licht, Adv. Energy Mat. 5 (2015) 1401491 1;
(c) H. Wu, Ji D, L. Li, D. Yuan, Y. Zhu, B. Wang, Zhang Z, S. Licht, Int. J. Adv. Mater. Technol. 5 (2016) 1600092 1.
[25] S. Licht, B. Wang, S. Ghosh, H. Ayub, D. Jiang, J. Ginley, J. Phys. Chem. Lett. 1 (2010) 2363–2368.
[26] S.W. Kim, K. Uematsu, K. Toda, M. Sato, J. Ceram. Soc. Jpn. 123 (5) (2015) 355.
[27] S. Lee, M. Kim, M. Hwang, K. Kim, C. Jeon, J. Song, Exp. Therm. Fluid Sci. 49 (2013) 94.
[28] W. Masschelein, Ozone 20 (2008) 191–193.
[29] C.E. Vaukal, Oxygen-Enhanced Combustion, Ed. CEC Press, Boca Tatonne, 1998 ISBN 0-8493.
[30] R. Hendershot, T. Lebrecht, M. Easterbrook, Chemical Eng. Progress (2010) July, 57 www.aiche.org/cep.
[31] F. Carrasco-Maldonado, J. Bakken, M. Ditaranto, N. Haugen, Ø. Langørgen, S. Grathwohla, J. Maier, Energy Procedia 120 (2017) 12.
[32] A. Contino, Fasilow F, Glass International, (2015) November.
[33] D. Leeson, N. Mac Dowell, N. Shah, C. Petit, P. Fennell, Int. J. Greenhouse Gas Control 61 (2017) 71.
[34] L.M. Farrell, T.T. Pavlack, L. Rich, Iron Steel Eng. 72 (3) (1995) 35.
[35] J. Von Schéele, Jenny Palm (Ed.), Energy Efficiency, InTech, 2010ISBN: 978-953-307-137-4.
[36] IEAGHG, Deployment of CCS in the Cement Industry, /19, December, 2013, at: (2013) https://hub.globalccsinstitute.com/publications/deployment-ccs-cement-industry/international-energy-agency.
[37] M.G. Ding, Z. Du, Prog.1995 Int. Conf. on Energy and Environment, Begell House, New York, Shanghai, China, 1995, p. 674.
[38] T. Banaszkiewicz, M. Chorowski, W. Gizicki, Energy Procedia 41 (2014) 127.
[39] Y. Alsultanny, N. Al-Shammari, Eng. J. 18 (2014) 67.
[40] M. Chorowski, W. Gizicki, Arch. Thermodyn. 36 (2015) 157.
[41] M.W. Chase, Thermodynamic data, J. Phys. Chem. Ref. Data 9 (1998) 1 data available at: http://webbook.nist.gov/chemistry/form-ser.html.
[42] S. Licht, B. Cui, J. Stuart, B. Wang, J. Lau, Energy Environ. Sci. 6 (2013) 3646.
[43] (a) P. Claes, D. Moyaux, D. Peeters, Eur. J. Inorg. Chem. 4 (1999) 583;
(b) D. Peeters, D. Moyaux, P. Claes, Eur. J. Inorg. Chem. 4 (1999) 589.